Int J Earth Sci (Geol Rundsch) (2005) 94: 990–1009
DOI 10.1007/s00531-005-0013-2

ORIGINAL PAPER

Volker Lüders · Christian Reutel · Peer Hoth
David A. Banks · Birgit Mingram · Thomas Pettke

Fluid and gas migration in the North German Basin: fluid inclusion and stable isotope constraints

Received: 20 October 2004 / Accepted: 14 April 2005 / Published online: 26 August 2005

Abstract Fluid inclusions have been studied in minerals infilling fissures (quartz, calcite, fluorite, anhydrite) hosted by Carboniferous and Permian strata from wells in the central and eastern part of the North German Basin in order to decipher the fluid and gas migration related to basin tectonics. The microthermometric data and the results of laser Raman spectroscopy reveal compelling evidence for multiple events of fluid migration. The fluid systems evolved from a H_2O–$NaCl \pm KCl$ type during early stage of basin subsidence to a H_2O–$NaCl$–$CaCl_2$ type during further burial. Locally, fluid inclusions are enriched in K, Cs, Li, B, Rb and other cations indicating intensive fluid–rock interaction of the saline brines with Lower Permian volcanic rocks or sediments. Fluid migration through Carboniferous sediments was often accompanied by the migration of gases. Aqueous fluid inclusions in quartz from fissures in Carboniferous sedimentary rocks are commonly associated with co-genetically trapped CH_4–CO_2 inclusions. *P*–*T* conditions estimated, via isochore construction, yield pressure conditions between 620 and 1,650 bar and temperatures between 170 and 300°C during fluid entrapment. The migration of CH_4-rich gases within the Carboniferous rocks can be related to the main stage of basin subsidence and stages of basin uplift. A different situation is recorded in fluid inclusions in fissure minerals hosted by Permian sandstones and carbonates: aqueous fluid inclusions in calcite, quartz, fluorite and anhydrite are always H_2O–$NaCl$–$CaCl_2$-rich and show homogenization temperatures between 120 and 180°C. Co-genetically trapped gas inclusions are generally less frequent. When present, they show variable N_2–CH_4 compositions but contain no CO_2. *P*–*T* reconstructions indicate low-pressure conditions during fluid entrapment, always below 500 bar. The entrapment of N_2–CH_4 inclusions seems to be related to phases of tectonic uplift during the Upper Cretaceous. A potential source for nitrogen in the inclusions and reservoirs is C_{org}-rich Carboniferous shales with high nitrogen content. Intensive interaction of brines with Carboniferous or even older shales is proposed from fluid inclusion data (enrichment in Li, Ba, Pb, Zn, Mg) and sulfur isotopic compositions of abundant anhydrite from fissures. The mainly light $\delta^{34}S$ values of the fissure anhydrites suggest that sulfate is either derived through oxidation and redeposition of biogenic sulfur or through mixing of SO_4^{2-}-rich formation waters with variable amounts of dissolved biogenic sulfide. An igneous source for nitrogen seems to be unlikely since these rocks have low total nitrogen content and, furthermore, even extremely altered volcanic rocks from the study area do not show a decrease in total nitrogen content.

V. Lüders (✉) · B. Mingram
GeoForschungsZentrum Potsdam,
Telegrafenberg, 14473 Potsdam, Germany
E-mail: volue@gfz-potsdam.de
Tel.: +49-331-2881434
Fax: +49-331-2881436

C. Reutel
Geowissenschaftliches Zentrum Göttingen,
Goldschmidtstr. 1-3, 37077 Göttingen, Germany

P. Hoth
Bundesanstalt für Geowissenschaften und Rohstoffe,
Dienstbereich Berlin, Wilhelmstraße 25-30,
13593 Berlin, Germany

D. A. Banks
School of Earth Sciences, University of Leeds,
LS29JT Leeds, UK

T. Pettke
Department of Earth Sciences,
Institute for Isotope Geochemistry and Mineral Resources,
ETH Zürich, Sonneggstr. 5, CH-8092 Zurich, Switzerland

Introduction

Primary fluid inclusions hosted in diagenetically formed minerals can record important information for the reconstruction of the thermal history through time within a sedimentary basin. As pointed out by Goldstein and Reynolds (1994), an important prerequisite

for a successful fluid inclusion study in sedimentary terrains is the careful analysis of paragenetic relationships of diagenetic minerals that formed at different stages of subsidence or uplift during basinal history and the petrography of fluid assemblages hosted therein. Under the best circumstances, the sources of fluids associated with oil and/or hydrocarbon migration can be traced by studies of the fluid inclusion compositions (e.g. microthermometry, crush-leach bulk analysis, laser ablation ICP-MS analysis, synchrotron radiation induced X-ray fluorescence microanalysis, laser Raman spectroscopy) and P–T–x conditions for fluid inclusion entrapment can be reconstructed. However, caution must be exercised because fluid inclusions can undergo post-entrapment changes that may lead to a large range in homogenization temperatures in the studied inclusions. Especially in highly mature basins with multiple stages of burial and inversion tectonics fluid inclusions in diagenetic minerals are often altered due to stretching, leakage, or necking-down (Roedder 1984) and therefore, the results of fluid inclusion microthermometry do not always allow a conclusive interpretation. A discussion on mechanisms for alteration of fluid inclusions including heterogeneous entrapment, necking-down after a phase change, thermal re-equilibration and nucleation metastability is given in great detail by, for example, Goldstein and Reynolds (1994) and Goldstein (2001).

This study focuses on fluid inclusions that are trapped in fissure minerals that precipitated due to fluid migration(s) in mature parts of the North German Basin (NGB) where gas accumulations are commonly hosted by Permian sandstones and/or carbonates. From the crosscutting relationships of fissures hosted by Palaeozoic sediments and evaporites and distinct mineral fillings therein, there is compelling evidence for multiple events of fluid migration related to basin tectonics. Our study aims to characterize the chemical composition of the migrating fluids and gases and to re-construct the P–T conditions of entrapment. A further main aim is to decipher the timing of migration of nitrogen-rich fluids into reservoirs in the eastern parts of the NGB. The data obtained are compared with previous results of fluid inclusion studies in the Lower Saxony Basin (Reutel et al. 1995).

Analytical procedure

The majority of the samples studied here originate from wells drilled in the central part and at the southeastern margin of the basin, the Altmark High, the Flechtingen–Calvörde Block as well as from the rim of the Mid German Crystalline High (Fig. 1).

Microthermometric measurements were conducted using a Fluid Inc. USGS heating–freezing system mounted on a BX50 Olympus microscope. The heating–freezing stage was calibrated with synthetic fluid inclusions supplied by Synflinc.

Gas-bearing inclusions were analysed with a Ramanor U-1000 (Jobin-Yvon) or a Jobin-Yvon LabRam Raman spectrometer. The exiting radiation used was a 514.5 nm Ar laser (Cohorent Innova 90-2) or 532 nm Nd/Yag laser, respectively.

Chemical analyses of the fluid inclusions in quartz, calcite and fluorite were carried out using the method outlined in detail in Banks et al. (2000). Samples of quartz, calcite and fluorite were crushed to approximately 1 mm and heated in 18.2 MΩ water to almost boiling, washed several times with similar quality water and the procedure was repeated. Dry samples between 0.5 and 1 g were crushed to a fine powder in an agate pestle and mortar, transferred to a sample container and 5–6 ml of 18.2 MΩ water was added to re-dissolve the dried salts. Prior to analysis, the samples were filtered through a 0.2-μm nylon filter. Anions were determined by Ion Chromatography and cations by Flame Emission Spectrometry. For both methods of analysis the typical precision was 5% RSD.

LA-ICP-MS analyses on individual fluid inclusions in samples from selected wells were performed at the ETH Zürich. The system at ETH Zürich consists of a pulsed 193-nm ArF Excimer laser (Lambda Physik, Germany) with an energy-homogenized (Microlas, Germany) beam profile (Günther et al. 1998) coupled with an ELAN6100 ICP quadrupole mass spectrometer (Perkin-Elmer, Canada). The laser system is characterized by a laterally homogeneous energy distribution, allowing depth-controlled ablation of material at a rate of 0.1–0.2 μm/shot, depending on laser energy and matrix chemistry. The resulting ablation craters are flat-bottomed and slightly conical. The optical imaging system design permits the use of different pit diameters (8–100 μm) at constant energy density on the sample, by adjusting an aperture in the laser-beam path. Simultaneous observation of the ablation process on the sample by a visual monitor and as real-time data signals is essential for controlled ablation of fluid inclusions. The sample was loaded along with the SRM 610 glass standard from NIST in a 1-cm^3 ablation cell and put on the stage of a modified petrographic microscope. Laser ablation aerosol was carried to the ICP-MS by a mixed He-Ar carrier gas. Analyses were performed in sequence, and each ablation was stored individually as transient (i.e. time resolved) signal acquired in peak-hopping mode. Two analyses on the external standard at the beginning and the end of each set, required for off-line data reduction, bracketed up to 16 analyses of unknowns. The certified glass standard SRM 610 was used as an external standard to calibrate analyte sensitivities, and bracketing standardization provided a linear drift correction. The analytical setup was tuned for optimum performance across the entire mass range. ICP-MS run conditions were very similar to those reported in Pettke et al. (2004). The analytical setup and data reduction scheme for fluid inclusions

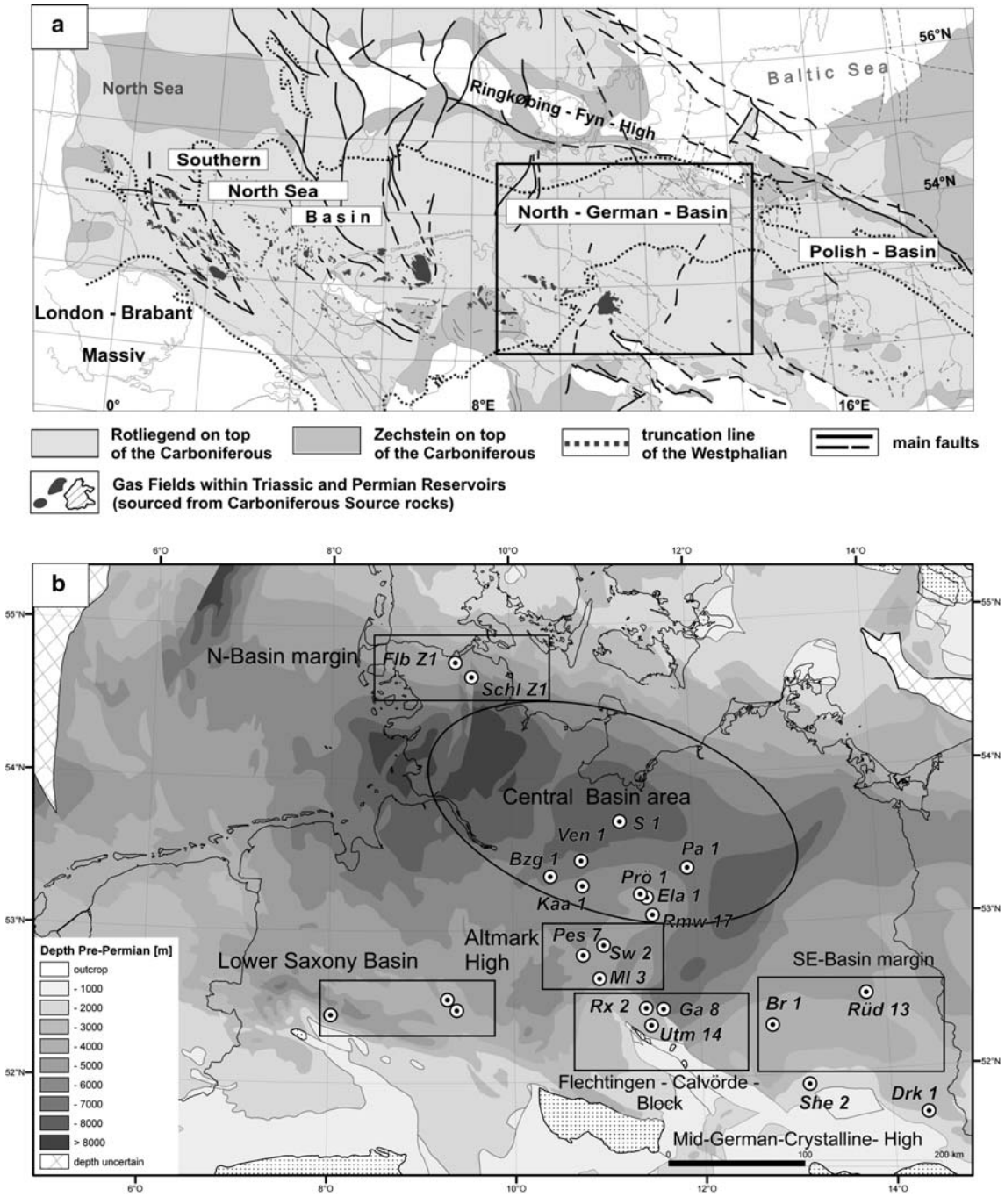

Fig. 1 **a** Location of the investigated area within the Mid-European Basin (outline of the basin area and location of the gas fields after Bandlowa 1998; the Northwest European Gas Atlas 1998; Hoth 1997). **b** Investigated regions of the North German Basin and locations of selected key wells (Depth of the Pre-Permian according to Gerling et al. 1999, the Northwest European Gas Atlas 1998 and Hoth 1997)

used here is described in great detail in Heinrich et al. (2003).

Sulfur isotopic analyses of sulfates were carried out on H_2S prepared by reaction at 350°C with Kiba solution. H_2S is precipitated as CdS, converted to Ag_2S and oxidized with V_2O_5 at 1,000°C to produce SO_2 that was used for the mass spectrometer measurements. Sulfur isotope ratios are reported as δ^{34} S relative to the Cañon Diablo Troilite (CDT).

Samples of Rotliegend volcanic rocks were analysed for fixed nitrogen content and nitrogen isotopic composition using 1 g of powdered rock samples that were digested in 40% HF for 7 days at room temperature using polypropylene bottles. After raising the pH by adding 20% KOH, the solution was distilled using a Kjeldahl apparatus and released ammonia was trapped in 0.1 N H_2SO_4. The amount of fixed-nitrogen was determined by titration. The N isotopic composition was

analysed on evaporated sulfates using an elemental analyser NA1500 coupled with a ConFlow II to a DELTAplus XL.

Results

Fluid inclusion petrography

Fissure mineralization hosted by Carboniferous shales, sandstones and greywackes consist of quartz, carbonates and, locally, anhydrite. At least two generations of quartz can be distinguished by crosscutting relationships, namely a milky quartz which is commonly associated with chlorite (quartz I), and a younger clear quartz (quartz II) that offsets fissures of quartz I. Locally, quartz I is overgrown by carbonates which are also offset or replaced by quartz II. Fissures filled with anhydrite do not contain any other minerals and, therefore, a paragenetic relationship to quartz or quartz–carbonate fissures is unclear.

Aqueous fluid inclusions in quartz have irregular or rounded shapes and sizes between 2 and 30 μm and, commonly, are associated with co-genetically trapped gaseous inclusions (Fig. 2a). Due to the high number of inclusions in the studied samples, a clear classification, i.e. primary versus secondary origin (Roedder 1984), is often vague or even impossible. Gaseous inclusions have always rounded elongated forms and are mostly larger in size (20–70 μm). In contrast, anhydrite and carbonates hosted by Carboniferous sediments only contain aqueous two-phase inclusions, >90% of which are of secondary origin. Primary fluid inclusions hosted in these minerals are typically orientated parallel to crystal planes. The size

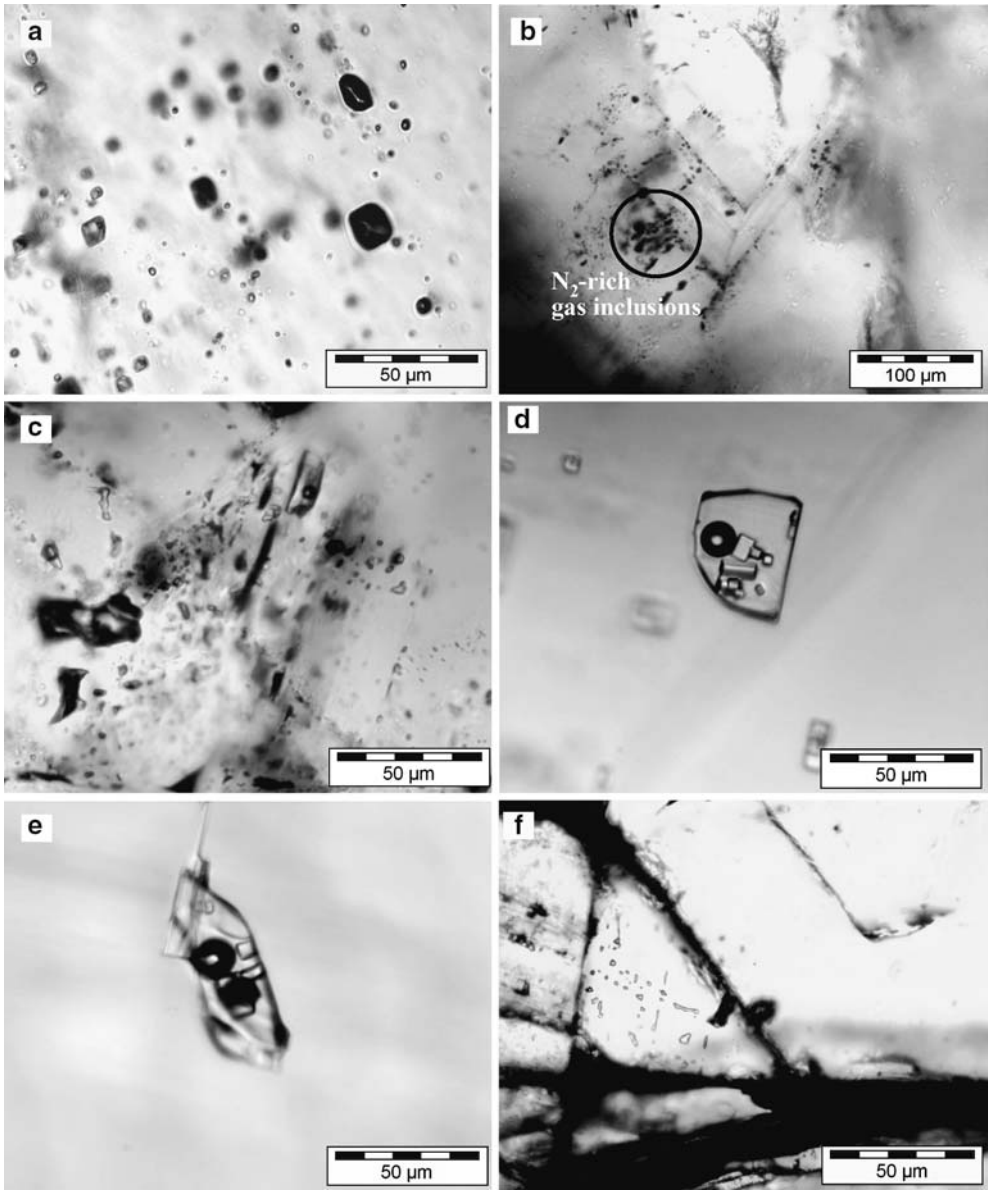

Fig. 2 Photomicrographs showing fluid and gas inclusions hosted in fissure minerals from wells in the North German Basin (*NGB*). (**a**) Cluster of aqueous two-phase inclusions and mono-phase CH_4/CO_2 gas inclusions in quartz hosted by Carboniferous greywake (Boizenburg). (**b**) Primary N_2-rich gas inclusions within growth zones in quartz hosted by a Permian vulcanite (Biegenbrück). (**c**) Quartz-hosted N_2-rich gas inclusions and co-genetically trapped aqueous two-phase inclusions (Biegenbrück). (**d**) Aqueous N_2-bearing (vapour phase) fluid inclusion with multiple daughter minerals of salts in calcite (Schwerin 1). (**e**) Aqueous, N_2-bearing fluid inclusion with daughter minerals of salts and hematite (?) in calcite (Schwerin 1). (**f**) Cluster of N_2/CH_4 gas inclusions in a octahedron plane of fluorite adjacent to older calcite (Uthmöden)

of primary fluid inclusions in the studied anhydrite and carbonate samples seldom exceeds 20 μm. The inclusions often exhibit irregular or even negative crystal forms.

The occurrence of quartz fissures in the studied sample material from Permian strata is restricted to volcanic rocks. The formation of quartz and/or agate nodules is most probably related to late magmatic fluid migration (Schmidt Mumm and Wolfgramm 2004). Fluid inclusions in quartz from nodules that probably precipitated at a late magmatic stage show highly variable liquid–vapour ratios probably due to variable formation temperatures. Quartz in fissures and veins that precipitated due to tectonically induced fluid migration is often associated with carbonates, and less frequently with fluorite and sulfides, in quarries in the Flechtingen-Calvörde Block. Locally, hematite occurs along with quartz or carbonates in fissures within the volcanic rocks. Anhydrite was only observed as infilling fissures within volcanic rocks in samples from wells that are drilled in the central parts of the basin (Fig. 1). Fluid inclusions, in the described fissure minerals, are mostly two-phase and are variable in shape and size, i.e. from some few microns up to 80 μm. Primary gaseous inclusions hosted in quartz were only observed in samples from 2 wells that were drilled in the basins centre and the southern margin, respectively. They occur in clusters or decorating growth zones and show rounded or irregular forms and sizes up to 40 μm (Fig. 2b, c). They are associated with only a few co-genetically trapped two-phase aqueous inclusions (Fig. 2c).

Fissures hosted by Rotliegend sediments are filled with carbonates or anhydrite. Both minerals contain numerous trails of secondary two-phase fluid inclusions. Fluid inclusions that can be classified as primary in origin are less frequent in the studied samples. When present, they are orientated parallel to crystal planes. Most of the primary inclusions are two-phase but locally small cubic daughter minerals, most probably halite can also be present in the inclusions. Calcite samples from fissures hosted by Rotliegend sandstones directly above the volcanic units of a well (S 1 in Fig. 1) in the central part of the basin contain multiphase inclusions, i.e. they consist of a liquid and a vapour phase and contain several solid inclusions (salts) or even small hexahedral hematite (?) crystals (Fig. 2d, e).

In the Flechtingen-Calvörde Block, some wells have penetrated hydrothermal vein mineralization of up to some 10 cm thickness. The vein fillings consist of anhydrite → calcite → fluorite (± chalcopyrite) → and locally barite. With the exception of sulfates, the mineral association calcite → fluorite (± chalcopyrite) resembles to those of calcite-fluorite veins which have been mined in the Lower Harz Mountains (Lüders and Möller 1992; Lüders et al. 1993; Stedingk et al. 1995). Gaseous inclusions (not being present in fluorite samples from the Harz Mountains) were only observed in some fluorite samples (Fig. 2f). Anhydrite and calcite host two-phase aqueous inclusions, whereas barite, the youngest mineral in the veins hosts mono-phase aqueous inclusions that show strong evidence for leakage and/or necking-down (indicated by huge vapour bubbles).

Some of these veins penetrate into overlying Zechstein carbonates (Ca 2) as well and have similar mineral assemblages (anhydrite → calcite → fluorite ± chalcopyrite). The fluid inclusion inventory is the same as described for vein minerals hosted by Rotliegend sediments. Similar to the veins in the underlying Rotliegend sandstones, gaseous inclusions are only present in fluorite that precipitated after anhydrite and calcite in the veins. Fissures and karst fillings in Zechstein carbonates consist of sparry calcite or locally anhydrite and host numerous secondary two-phase inclusions. Scarce primary fluid inclusions in calcite and anhydrite are also two-phase aqueous or may contain additionally halite daughter crystals.

Microthermometry

Aqueous inclusions

With the exception of fluid inclusions in milky quartz I from some fissures hosted by Pre-Permian sediments that show eutectic melting temperatures (Te) between −32 and −19°C, which are indicative for NaCl ± $MgCl_2$ fluids, all other measured fluid inclusions are characterized by low Te values ranging from −46°C down to −81°C (Appendix, Table 4). The final ice melting temperatures (Tm ice) in the latter inclusions lie commonly below −20.8°C (Appendix, Table 4), i.e. the eutectic of the system H_2O–NaCl, and point to high salinities and the presence of additional cations in the trapped liquids. Coupled melting of ice and a salt hydrate can be observed in some of these high-salinity inclusions, but often only metastable phase transitions (i.e. non-appearance of the hydrate phase and coupled lowering of the final ice melting temperatures) are visible.

The observed low-temperature phase transitions are comparable to the experimental data of Davis et al. (1990) and Spencer et al. (1990) and indicate NaCl and $CaCl_2$ to be major components in the fluids. In the ternary diagram (Fig. 3), fluid inclusions without halite daughter minerals in fissure minerals hosted by Carboniferous and Permian rocks plot along the cotectic line hydrohalite/halite, where most of the inclusions plot into the stability field of halite. A reason for this shift to higher salt concentrations may be the presence of additional cations in the trapped fluids. On the other hand, this shift can be related to metastable melting behaviour which is often observed in the system H_2O–NaCl–$CaCl_2$ (Spencer et al. 1990). Generally, coupled melting of hydrohalite and ice in fluid inclusions hosted in fissure minerals yield salinity of about 25–33 NaCl–$CaCl_2$ equiv.wt.% (Fig. 3) and variable cation content of 4.9–18 NaCl equiv.wt.% and 7–28.4 $CaCl_2$ equiv.wt.%, respectively. Fluid inclusions in fissure minerals hosted by Zechstein evaporates tend to have a higher $CaCl_2$

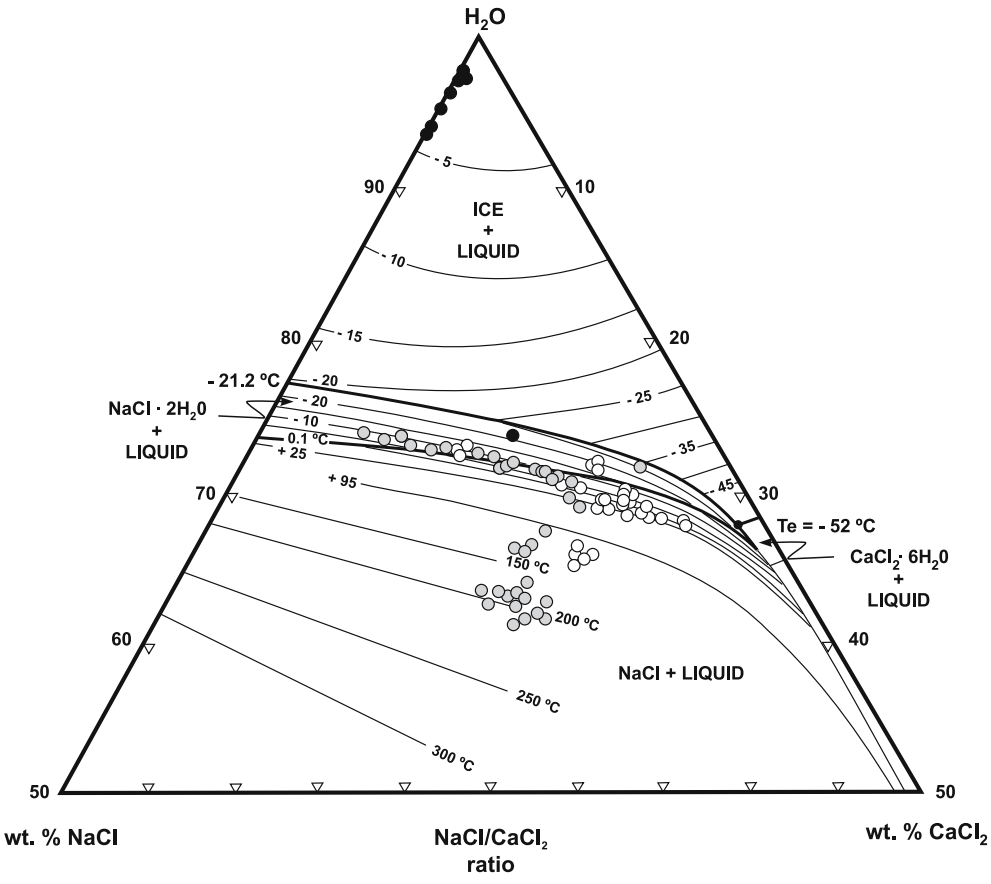

Fig. 3 H_2O–NaCl–$CaCl_2$ ratios of high-salinity fluid inclusions in fissure minerals. (Key to symbols: Carboniferous (*black*), Rotliegend (*grey*), Zechstein (*white*)

content (17.9–28.4 $CaCl_2$ equiv.wt.%) when compared with fluid inclusions in fissure minerals hosted by Rotliegend rocks (7–20 $CaCl_2$ equiv.wt.%). Probably, the mineral-forming fluids originated directly from Zechstein units or have altered evaporites (i.e. anhydrite or gypsum). Only individual inclusions hosted in samples from the Altmark High have a higher salinity between 36–39 NaCl–$CaCl_2$ equiv.wt.% (Fig. 3). An exception to the general trend of high salinity is recorded in fluid inclusions in milky quartz (quartz I) from the Boizenburg well in the central part of the basin (Appendix, Table 4). The Te values of these inclusions fall into a narrow range between −22 and −20.5°C and point to a predominantly H_2O–NaCl composition of the fluids and salinity between 9.8 and 16.5 NaCl equiv.wt.%.

The majority of the Te data (Appendix, Table 4) which are below the stable eutectic (−54.4°C) of the pure system H_2O–NaCl–$CaCl_2$ are difficult to interpret. Therefore, crush-leach bulk analysis and laser ablation ICP-MS (LA-ICP-MS) analysis on individual fluid inclusions in fissure minerals from selected wells have been carried out in order to obtain information about the chemistry of the trapped fluids. The results of the crush-leach analysis and LA-ICP-MS analysis are summarized in Table. 1, 2.

All investigated two-phase fluid inclusions homogenize into the liquid phase. When present, melting of halite daughter crystals mostly occurs prior to the homogenization of the vapour phase. Most homogenization temperatures (Th) range between 100 and 230°C (Appendix, Table 4). The highest homogenization temperatures were measured in fluid inclusions in chlorite-bearing quartz from a fissure hosted by Carboniferous sandstones from a well close to the Mid German Crystalline High (Drk 1, Appendix, Table 4). It is noteworthy that these inclusions show a H_2O–NaCl composition (Fig. 3) and therefore, quartz precipitation is related to an earlier fluid migration event. A trend of higher Th and lower Tm ice was also observed for fluid inclusions in several chlorite-bearing quartz (I) samples hosted by Carboniferous sediments from wells in other parts of the basin (Appendix, Table 4). Schmidt Mumm and Wolfgramm (2004) suggest that the migration of H_2O–NaCl dominated fluids is related to the waning stages of the Permo-Carboniferous magmatic event. Younger quartz (II) samples within the same well contain high-salinity fluid inclusions (Fig. 3) that homogenize between 100 and 125°C.

The homogenization temperatures only represent the minimum temperatures of entrapment. Since the homogenization of a two-phase inclusion occurs along the liquid–vapour curve and than follows the isochore slope which depends on the physico-chemical character of the inclusion, there can be a large difference between the measured Th and the true trapping temperature. On the other hand, fluid inclusions in quartz and/or car-

Table 1 Crush-leach and LA-ICP-MS analyses of fluid inclusions hosted by different minerals in fissures from well in the NGB. Anion and cation data obtained by crush-leach analyses reported in ppb (as analysed); *NA* not analysed

Crush-leach								
Sample	Mineral	Stratigraphy	F	Cl	Br	Na	K	Li
Parchim	Quartz	Upper Carboniferous	NA	133329	65	5445	283	7.3
Wardenburg	Fluorite	Zechstein	1572	19031	7.7	7161	783	130
Uthmöden	Fluorite	Zechstein	NA	41510	242	14223	1902	99
Uthmöden	Calcite	Zechstein	1700	65882	305	28776	3720	236
Vellahn 24	Calcite	Rotliegend	2052	47583	62	16016	1156	40
Eldena 29	Quartz	Upper Carboniferous	462	65516	563	27148	2744	204
DRK 66	Quartz	Carboniferous	572	7987	38	3839	937	20
SW-4	Calcite	Rotliegend	114	6892	1.9	2299	881	53
Vellahn V-19	Calcite	Rotliegend	163	8355	1.2	2849	2274	20
Bb 10	Quartz	Rotliegend volcanites	373	7832	54	2039	2083	15

Table 2 LA-ICP-MS analyses of individual fluid inclusions in calcite hosted by Rotliegend sandstones directly overlying volcanic rocks (Schwerin Z1) and 2 generations of quartz hosted by Carboniferous sandstones (Boizenburg 1)

FI#	Li 7	B 11	Na 23	Mg 25	P 31	K 39	Ca 42	Mn 55	Zn 66	As 75	Rb 85	Cs 133	Ba 137	Pb 208
S 1/1	791	433	119261	114	< 100	17671	NA	1575	631	22	184	73	NA	560
S 1/2	1150	314	116763	173	< 228	24334	NA	1822	695	< 14	229	105	NA	506
S 1/3	1121	367	116944	232	< 230	23850	NA	1743	840	< 16	306	177	NA	560
S 1/4	1274	645	116041	287	< 850	26257	NA	3720	916	93	234	95	NA	439
S 1/5	3142	793	110125	513	3822	42035	NA	3319	1811	94	488	245	NA	150
S 1/6	834	311	119191	637	< 514	17859	NA	1408	554	< 34	259	85	NA	581
S 1/7	1138	1346	115488	572	< 1047	27734	NA	2672	887	< 68	307	120	NA	678
S 1/8	1368	471	118119	206	< 142	20718	NA	1711	685	14	239	116	NA	513
S 1/9	1566	605	115825	240	< 261	26834	NA	2362	1117	42	330	145	NA	627
S 1/10	1888	573	114390	449	< 253	30663	NA	2238	1059	22	280	200	NA	209
S 1/11	1392	735	118455	945	1406	19820	NA	1883	1209	51	259	122	NA	670
S 1/12	1074	349	119689	187	259	16531	NA	2080	596	21	185	86	NA	528
S 1/13	1443	423	117388	267	194	22666	NA	1948	804	20	240	110	NA	478
S 1/14	1275	395	117879	263	< 192	21359	NA	1879	933	20	216	104	NA	577
Bzg quartz I-1	10985	289	58518	487	2504	2046	15340	146	281	< 46	< 10	12	460	71
Bzg quartz I-2	19177	< 300	58846	< 475	4732	1687	< 31775	252	395	118	< 31	14	526	77
Bzg quartz I-3	17797	< 443	53321	569	5503	1014	< 30097	174	353	< 140	< 30	12	555	81
Bzg quartz II-1	2350	< 109	83491	1681	1183	718	63355	917	6464	< 50	< 11	< 3	5044	2257
Bzg quartz II-2	2194	456	87791	2112	< 2269	704	55466	818	6238	< 165	< 29	< 10	4052	1653
Bzg quartz II-3	28809	601	80373	2368	10474	951	69078	677	6933	< 159	< 41	< 10	5010	1743
Bzg quartz II-4	6431	< 238	79647	2379	1957	< 545	70409	1200	8470	< 117	< 24	< 10	6649	2116
Bzg quartz II-5	13657	141	87575	2319	3927	747	55862	789	6744	< 39	21	4	4150	2019

Values following the element indicate the isotope analysed. All concentrations are reported in microgram per gram. For values below the limit of detection, the limit of detection is given, marked as "< value >" (calculated as 3 standard deviations of the background divided by sensitivity). *NA* not available (signals dominated by host calcite)

bonate cements that precipitated from pore fluids during diagenesis can record important information about the thermal gradient at the time of entrapment, if the pore fluids have achieved thermal equilibrium with the host rocks. This has been demonstrated by Rieken (1988) for some Rotliegend boreholes in the Lower Saxony Basin. The homogenization temperatures of fluid inclusions in fissure minerals from boreholes in the central basin area (Fig. 1) show no general trend of increasing temperature with depth, with respect to present-day burial depth (Fig. 4). This indicates that the mineral-forming fluids have not (always?) achieved thermal equilibrium with the host rocks or, perhaps, that multiple events of fluid migration and mineral precipitation occurred within the same drill core at different times. This assumption is also indicated by the crosscutting relationships of distinct fissure minerals (i.e. quartz I → carbonate → quartz II). Multiple fluid migration within the NGB has also been suggested by, for example, Rieken (1988), Rieken and Gaupp (1991), Reutel and Lüders (1998), Lüders et al. (1999), Wolfgramm (2002), Schmidt Mumm and Wolfgramm (2004).

Gas inclusions

The occurrence of gas-bearing inclusions is very heterogeneous in the studied samples. In some samples the frequency of gaseous inclusions exceeds those of aqueous inclusions many times, other samples only contain a

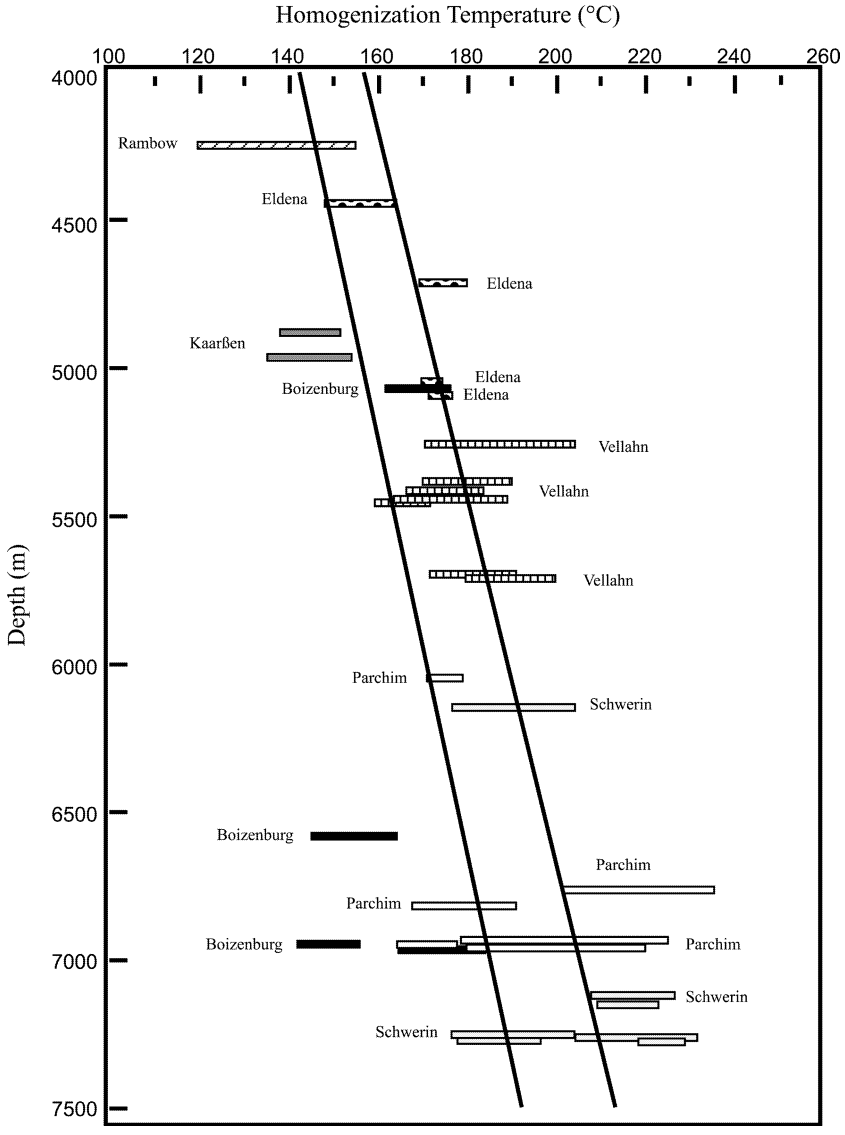

Fig. 4 Homogenization temperatures versus depth diagram for wells in the central part of the basin.

few gaseous inclusions and a high frequency of aqueous inclusions. In most samples there is evidence of contemporaneous trapping of aqueous and gas inclusions as indicated by the occurrence of both types of inclusions in same clusters and/or growth zones. Gaseous inclusions mostly show no visible rim of water and appear monophase at room temperature (Fig. 2a, c, f). They were observed in samples hosted by all the studied stratigraphic units (i.e. Carboniferous to Zechstein). Raman spectroscopic analysis proves that there to be two compositional types of gaseous inclusions in general: (1) CH_4-rich gas inclusions with variable amounts of CO_2 or N_2 with CH_4 content >75 mol%, and (2) N_2-rich inclusions with variable CH_4 content but $<$ 40 mol% (Fig. 5).

H_2S-rich inclusions with variable H_2S content (18–76 mol%) that are reported from calcite and fluorite hosted by Zechstein carbonates from the Lower Saxony Basin (Fig. 1) were not observed in the studied samples. The origin of H_2S in inclusions from the Lower Saxony Basin is related to partial thermochemical sulfate reduction within the Zechstein evaporites (Reutel et al. 1995).

The occurrence of CH_4-rich inclusions in the studied samples is commonly restricted to minerals hosted by Carboniferous rocks or, in one case, to fissure minerals hosted by Lower Zechstein shales (Kupferschiefer). N_2-rich inclusions occur in minerals hosted by Permian volcanic rocks and sandstones as well as in Zechstein carbonates, mudstones or within Zechstein anhydrite (A1).

During freezing and re-heating runs CH_4-rich inclusions commonly show melting of a solid phase (CO_2) in the temperature range between -110 and -64°C followed by V $\rightarrow$ L homogenization of CH_4 in the temperature range between -90 and -53°C (Appendix, Table 4). In contrast, most of the N_2-rich inclusions commonly hosted in fluorite or quartz homogenize into the vapour phase indicating high molar volumes of the trapped gases (Thiéry et al. 1994). Only N_2-rich inclusions in quartz hosted by a magmatic dyke within the

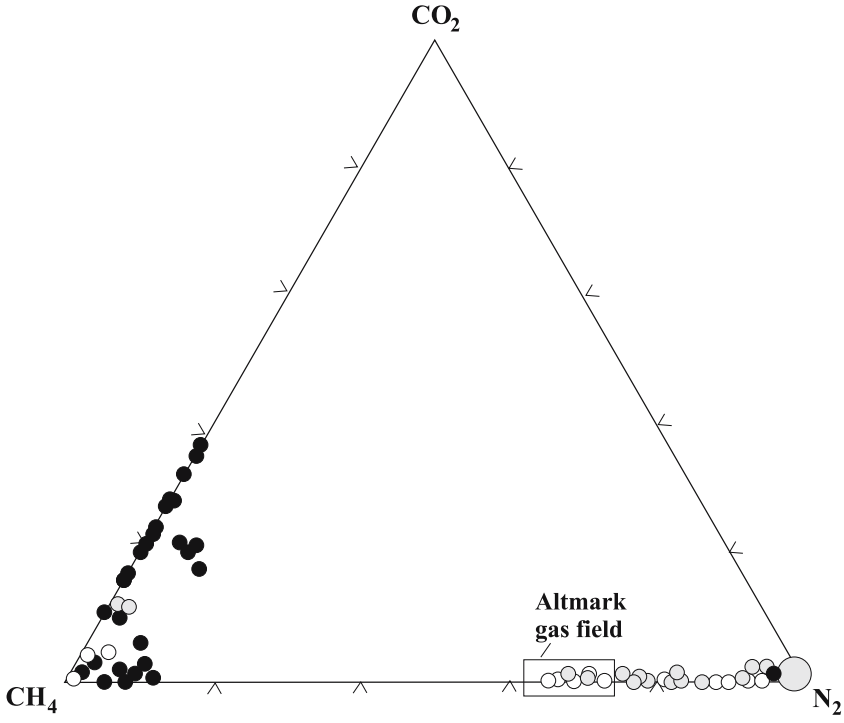

Fig. 5 Raman composition of gaseous inclusions in samples from investigated wells. Carboniferous (*black*), Rotliegend (*grey*), Zechstein (*white*)

Table 3 Fixed nitrogen content and δ15N isotopic composition of Permian volcanic rocks from quarries in the Flechtingen Block

Locality	Sample no	Rock type		NH_4-N (ppm)	$\delta^{15}N_{fix}$ [‰]
Bodendorf	FH1	Andesitoid		45	12.3
	FH4a	Andesitoid		116	6.2
	FH4b	Andesitoid	Altered	39	8.1
Eiche	FH8	Andesitoid	Altered	29	7.6
	FH10	Andesitoid	Altered	35	9.4
Flechtingen	FH12	Ignimbrite		108	13.5
	FH13	Ignimbrite		88	13.3
	FH14	Ignimbrite		76	12.9
	FH15	Ignimbrite		102	14.4
	FH16	Ignimbrite		23	15.4

Schleswig Z1 well (Schl Z1 in Fig. 1) show V → L homogenization in the temperature range between −148.6 and −146.5°C. Here, N_2–CH_4-bearing inclusions are co-genetically trapped in a small quartz vein within a magmatic dike that penetrates Carboniferous shales. N_2-bearing inclusions were also found in a calcite vein hosted by lowermost Rotliegend sandstones from the Schwerin 1 well in the central basin (S 1 in Fig. 1). These inclusions contain several daughter crystals of salts and a vapour phase (Fig. 2d) which contain considerable amounts of N_2 as indicated by Raman spectroscopy (Fig. 5). The homogenization temperatures of these inclusions are between 205 and 232°C (Table. 1, 2). The liquid phase has high Na, K, Li. Cs, B, Rb and metal content (Table. 1, 2) which may be indicative of intensive interaction of the saline brines with volcanic rocks. It cannot be excluded that N_2 content in the described inclusions is derived by thermal overprint of Carboniferous shales (Schleswig Z1) or alteration of underlying volcanic rocks (Schwerin 1).

Crush-leach and LA-ICP-MS analysis

The halogen content of the fluid inclusions can be used to discriminate between different fluids and provide information on their origin. The Cl and Br content of fluids are not affected by water–rock interactions (WRIs) except where the dissolution or precipitation of evaporites (halite, sylvite, etc.) are involved. However, the involvement of Cl evaporites is unambiguous and can easily be determined using halogen ratios. Evaporation of seawater to halite saturation does not change the Cl/Br(m) ratio of *c*. 655, during halite precipitation the ratio in the fluid decreases to *c*. 240 at the point where halite ceases to precipitate. Further evaporation leads to even more Br-rich fluids. Dissolution of halite can produce a large range in Cl/Br(m) ratios from *c*. 20,000 to 5,000 as the Br content of the halite increases from around 65 ppm for the initial halite to ca. 300 ppm at the end of halite precipitation (Fontes and Matray 1993).

The fluids in this study fall into two distinct groups (Fig. 6) with the majority having Cl–Br ratios less than that of seawater, and lying on or close to the region where halite precipitates from evaporating seawater. The other group has a large range of Cl–Br ratios from ca. 2,000 to 16,000 that can only result from halite dissolution. The different samples all lie on the same line, indicating mixing of two fluids in different proportions. However, it is clear that the high Cl-fluid, although representing halite dissolution, does not come close to intersecting halite on either Fig. 6 or 7. In the former the fluid inclusions all plot well to the left of the line for halite dissolution and indicate loss of Na due to WRI. Similarly in Fig. 7, the fluid inclusions plot on a vertical line that intersects the more evolved Br-rich fluid and does not go towards halite. The variation in Cl/Br with constant Na/Cl is consistent with mixing of the Br-rich fluids with a halite dissolution brine that has undergone extensive WRI and exchange of Na for other cations. For example, this could be Ca if interaction with plagioclase is involved (Davisson and Criss 1996) or K if albitisation of K-feldspar has taken place (Banks et al. 2002). The more evolved brines also show evidence of loss of Na by WRI as in both the above figures some of the fluid inclusions plot to the left of the seawater evaporation line. The magnitude of Na loss is much greater in the halite-derived end-member fluid than in the Br-rich brines as shown by the significantly lower Na–Br and Na–Cl ratios than those expected for mixing a halite dissolution brine and one from evaporated seawater from which halite had precipitated.

The extent of WRI and Na–K alteration is more clearly seen in Fig. 8. Some of the Br-rich fluids are on

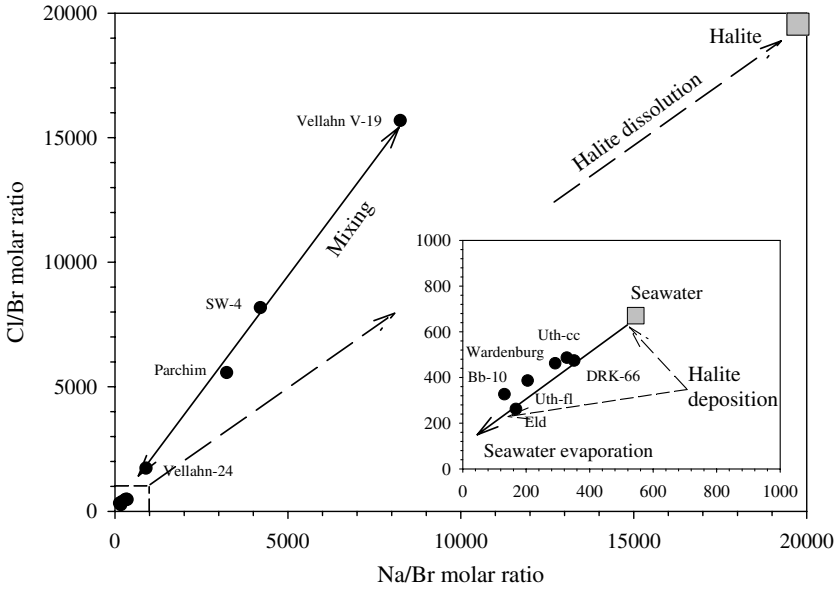

Fig. 6 Na/Br and Cl/Br molar ratios of inclusion fluids relative to evaporation of seawater and dissolution of halite. The inclusion fluids fall into two groups either derived from dissolution of halite or from the residual brine remaining after halite has precipitated from seawater

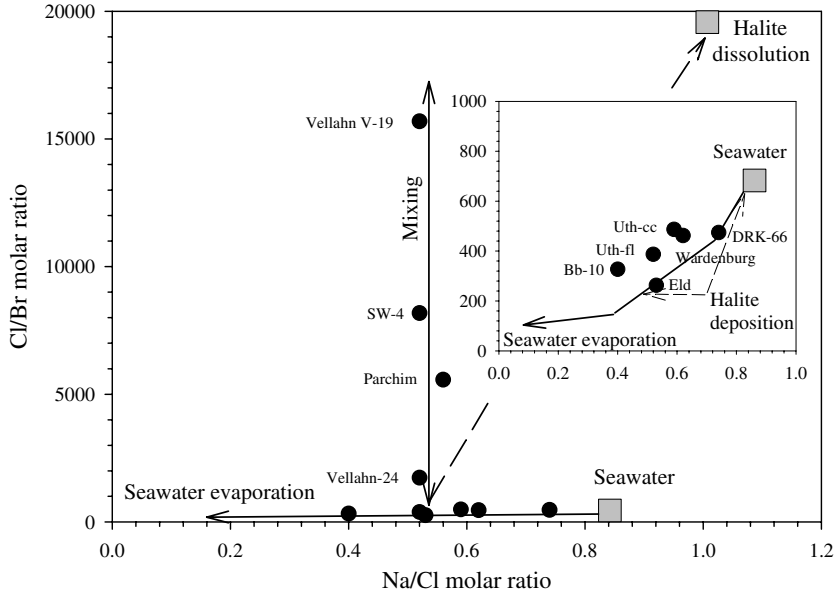

Fig. 7 Na/Cl and Cl/Br molar ratios of the inclusion fluids. The *vertical mixing line*, at a constant Na/Cl ratio of ca. 0.5, reveals the extent of Na loss from the halite dissolution fluid

or close to the seawater evaporation line and, although they exhibit different Na–K ratios, the values are consistent with their degree of evaporation as defined by their Cl–Br ratios. Others are further to the left reflecting a significant degree of alteration. The fluid inclusions with the variable amounts of the halite dissolution fluid should have increasing Na–K ratios as the Cl–Br ratio increases, i.e. more of the halite-derived fluid. In fact they show the opposite with decreasing Na–K ratios as the Cl–Br ratio increases. This is accounted for by the halite dissolution fluid having undergone extensive WRI, losing significant Na and resulting in the end-member fluid having a Na–K ratio of *c*. 1–2. Mixing with the other, Br-rich end-member fluid with Na–K ratio of *c*. 25 would produce the observed decrease of Na–K with increasing Cl–Br. The vertical mixing line in Fig. 7 at a Na–Cl ratio of *c*. 0.5 instead of higher ratios, that would be determined by the degree of mixing along a line that goes towards halite where the Na/Cl ratio is 1.0, shows that approximately 50% of the expected Na has been lost from the halite end-member fluid.

The WRI has not resulted in a fluid that is in equilibrium with sedimentary and/or crystalline rocks it interacted with. Using the Na–K and Na–Li geothermometers of Verma and Santoyo (1997) and the fluid analyses Fig. 9, it can be seen that the two geothermometers give not only widely differing temperatures, but temperatures that are unrealistically high. The majority of fluids have Na–Li ratios that give temperatures of between 400 and 500°C and Na/K ratios that give temperatures from 500 to 200°C. However, the majority of the fluids have essentially the same Na/Li ratio of *c*. 50 which represents a substantial increase from the Na/Li of Br-rich brines, whose maximum Na/Li is ca. 6,500 and of halite ca. 55,000 (Fontes and Matray 1993). The major repository for Li is in micas and such a major increase in the fluid concentration of high-salinity brines must indicate significant destruction of these minerals by WRI.

LA-ICP-MS analyses have been performed on individual fluid inclusions hosted in calcite and two generations of quartz (Table. 1, 2). The analysed calcite sample originates from the Schwerin 1 well (Fig. 1) and is hosted by Rotliegend sandstone directly overlying volcanic rocks at a depth of 7,256.9 m. The trapped inclusions in this sample show multiple daughter crystals as well as nitrogen content in the vapour bubble (Fig. 2d, e). The fluid is characterized by elevated B, K, Cs and Rb content when compared with quartz-hosted inclusions from Upper Carboniferous strata (Table. 1, 2). An intriguing explanation for this unusual composition might be intensive WRI by brines with the underlying volcanic rocks. It cannot be excluded that the rocks nitrogen detected in the vapour bubble was derived from alteration of ammonia-bearing mica or feldspars in the volcanic rocks. However, it is noteworthy that the analysed inclusions are unique because other calcites from the same drill core contain inclusions that do not have any detectable nitrogen in their vapour bubbles and do not contain abundant daughter crystals.

Fluid inclusions in two generations of quartz (quartz I and II) hosted by Upper Carboniferous sandstones from the Boizenburg drill core show a distinctly different chemical composition (Table. 1, 2). Quartz I, which is associated with chlorite, hosts inclusions that have high Li and Na concentrations and considerable amounts of K and traces of Cs. In contrast, fluid inclusions in quartz II, that crosscuts quartz I, has higher Na, Ca and Mg concentrations. Furthermore, the inclusions also contain significantly higher concentrations of Ba, Pb, Zn and Mn, but lower K when compared with inclusions in the older quartz (Table. 1, 2). This shows that during basin evolution, progressive alteration of deeply buried sedimentary rocks by saline fluids must have occurred. The high Ba and metal concentrations probably indicate

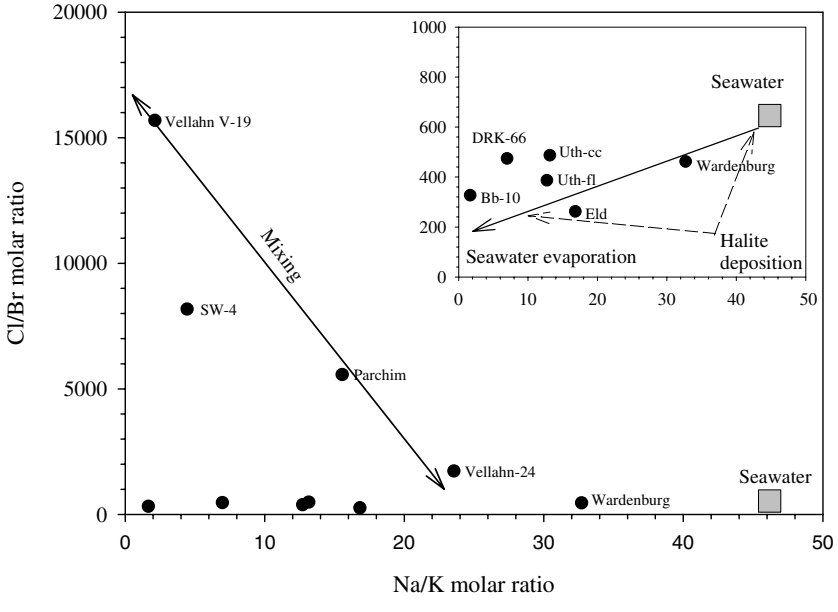

Fig. 8 Na/K and Cl/Br ratios of the fluid inclusions. The difference from the expected Na/K ratios of evaporating seawater is variable, with some of the fluids showing little or no difference

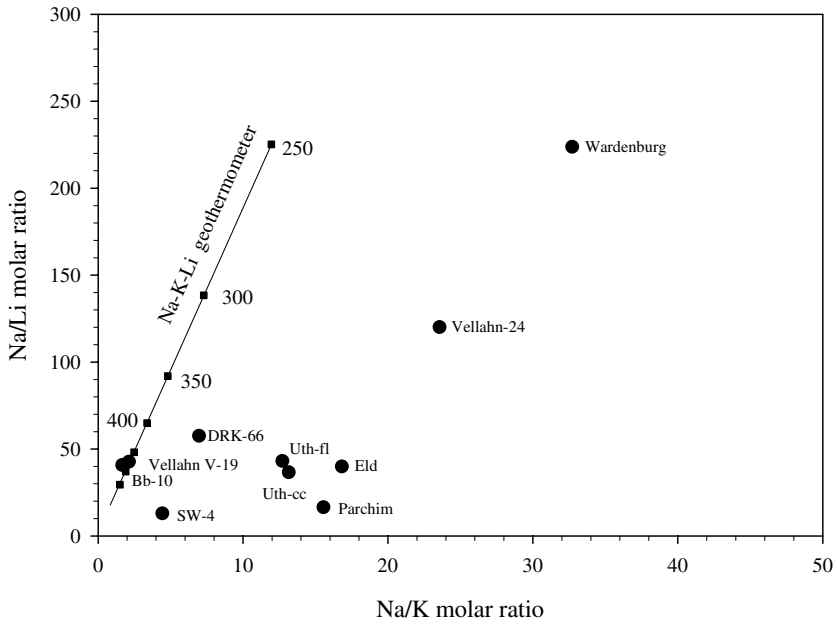

Fig. 9 Na/K and Na/Li molar ratios of the fluid inclusions relative to the Na–K and Na–Li geothermometers. The Na–K–Li composition of the fluids indicate variable and in the case of Na/Li unrealistically high temperatures. The fluids appear not to be in equilibrium with crystalline rocks with which they interacted

WRI between the brines and shales that are normally enriched in these elements.

Sulfur isotopes of anhydrite

The sulfur isotopic composition has been measured in 31 samples of anhydrite from fissure mineralization. The $\delta^{34}S$ values are highly variable and are either negative or positive (Fig. 10). Also, the $\delta^{34}S$ values of anhydrite samples from the same well can be very heterogeneous. For example, the most negative value (−20.69 ‰) was obtained for an anhydrite sample from a fissure hosted by Lower Carboniferous shales from the Schleswig Z1 drill core. Two other samples from the drill core have considerably different $\delta^{34}S$ values (+4.35‰ and +16.03‰) and either suggest different sources for sulfate or that anhydrite precipitated under quite different physico-chemical conditions; i.e. changes in pH and oxygen fugacity (Ohmoto 1972). Although changes in fO_2 and pH can cause large variations in sulfur isotopic composition (Ohmoto and Lasaga 1982) it is very unlikely that anhydrite formation resulted from a uniform fluid source within a huge basin because fluid inclusions in anhydrite show very heterogeneous ranges for Th and Tm_{ice} values (Appendix, Table 4). Therefore, the observed variations in the sulfur isotopic compositions of the fissure anhydrites more likely indicate different sources of sulfate. The large negative $\delta^{34}S$ values of some anhydrite samples can be derived through oxidation and re-deposition of biogenic sulfide sulfur. In this respect, one source of sulfur can be assumed to be sedimentary sulfides. Positive $\delta^{34}S$ values between +16 and +23.7‰ indicate an origin of sulfate from (Pre-Permian or Triassic) formation waters. A pristine Zechstein origin can be excluded due to the lower $\delta^{34}S$ values (+10 to +13‰) of Zechstein ocean water or evaporites (Nielsen 1979). For a Zechstein origin of the sulfate, the heavier $\delta^{34}S$ values can only be ex-

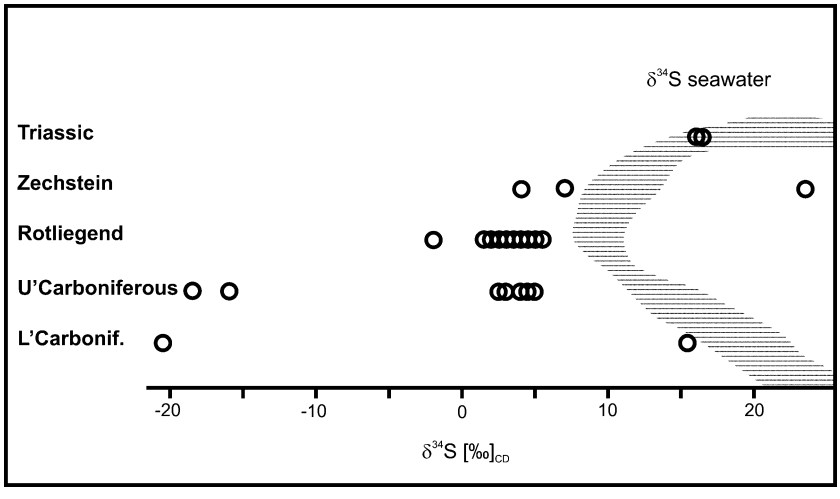

Fig. 10 Sulfur isotopic composition of anhydrites from fissures in different stratigraphic units. Most of the samples plot left from the paleo seawater line, indicating that the anhydrites did not gain their sulfur content purely from formation waters (*for details see text*)

plained by fractionation processes such as partial sulfate reduction. The $\delta^{34}S$ values between −2 and +8‰ suggest mixing of SO_4^{2-} dominant formation waters with variable amounts of dissolved biogenic sulfide. On the other hand, δ^{34} S between 0 and +3‰ may also be derived by alteration of igneous sulfide.

Discussion

Fluid evolution

Studies of fluid inclusions in minerals hosted by Carboniferous and Permian rocks have revealed a complex fluid evolution and evidence for multiple stages of fluid and gas migration in the NGB. The chemical analyses of high-salinity fluid inclusions showed that at least two distinct fluid types that have mixed in variable proportions. The majority of the fluid inclusions represent seawater that has evaporated past halite saturation and has undergone WRI losing Na and gaining K as well as other cations. The degree of Na loss of this end-member fluid was not large and some fluids show little evidence of it. The other group of fluid inclusions contain fluids with Cl/Br ratios that are substantially greater than that of seawater, which can only come from dissolution of halite. Different samples have different Cl/Br ratios that indicate mixing of the evaporated brine and the halite dissolution fluid in different proportions. The mixing trends show that this end-member fluid does not have the composition expected if pure halite were dissolved. Prior to mixing of the two fluids, the halite dissolution fluid lost approximately 50% of its Na and gained K to produce a fluid with a Na/K ratio of ca.1, and it is this fluid that mixed with the evaporative brine. However, the fluids appear not to have equilibrated with the sedimentary and/or crystalline rocks they interacted with.

Aqueous fluid inclusions in at least two quartz generations hosted by Carboniferous sediments are commonly associated with CH_4–CO_2 inclusions and developed from an H_2O–NaCl fluid in quartz I through a H_2O–NaCl–$CaCl_2$ composition in quartz II as indicated by LA-ICP-MS analyses (Table. 1, 2). In general, the Th values of fluid inclusions in early quartz range between 150 and 230°C, whereas in younger quartz they do not exceed 200°C and the CO_2 content in co-genetically trapped gaseous inclusions increases. Fluid inclusion petrography has shown compelling evidence for co-genetic entrapment of aqueous and gaseous inclusions in fissure minerals from wells in the NGB and therefore, *P–T* conditions during fluid entrapment via isochoric *P–T* projections can be reconstructed (Fig. 11). From the isochoric *P–T* sections it turns out that trapping of aqueous and CH_4–CO_2 inclusions occurred at pressures between 600 and 1,500 bar.

For individual wells in the central basin area where at least two generations of quartz can be distinguished, due to the crosscutting relationships of fissures and/or mineral assemblages, the pressure conditions of inclusion entrapment are heterogeneous for quartz I and quartz II. For example, a sample from the Boizenburg drill core, which penetrated into a Carboniferous trough, exhibits two generations of quartz (quartz I and II) at 6,940 m depth. Fluid inclusions in quartz I were trapped under a pressure regime of about of about 800 bar, whereas fluid inclusions in quartz II yield higher pressures of about 1,200– 1,500 bar (Fig. 12), indicating that within this well at least two events of fluid and gas migration are recorded. Due to the considerable difference in pressure it seems plausible that the migration of fluids and gas are related to different stages of basin evolution and thus, occurred at different times. Under a hydrostatic pressure regime quartz I would have precipitated at about 8 km depth and quartz II between 12 and 14-km depth, which appears unrealistic because this would require erosion after entrapment of at least 7 km. Considering the lithostatic pressure conditions during fluid entrapment, quartz I would have precipitated at a

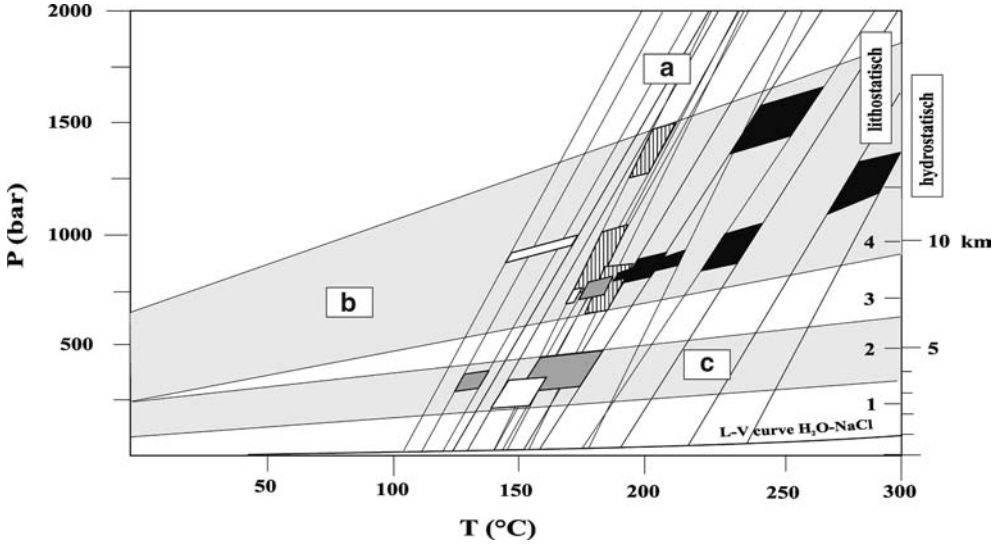

Fig. 11 *P–T* diagram showing trapping conditions of primary co-genetic aqueous (**a**) and CH_4/CO_2 (**b**) and N_2/CH_4 (**c**) inclusions from selected samples via isochore construction. Isochores were calculated with the MacFlinCor computer programme (*Brown* and Hagemann 1994). *P–T* conditions of entrapment are shown as *shaded areas*. Carboniferous (*black*), Rotliegend (*grey*), Zechstein (*white*). *Hatched fields* show *P–T* trapping conditions of co-genetic aqueous and CH_4-rich gas inclusions in quartz hosted by Carboniferous rocks from wells of the Lower Saxony Basin (Reutel et al. 1995)

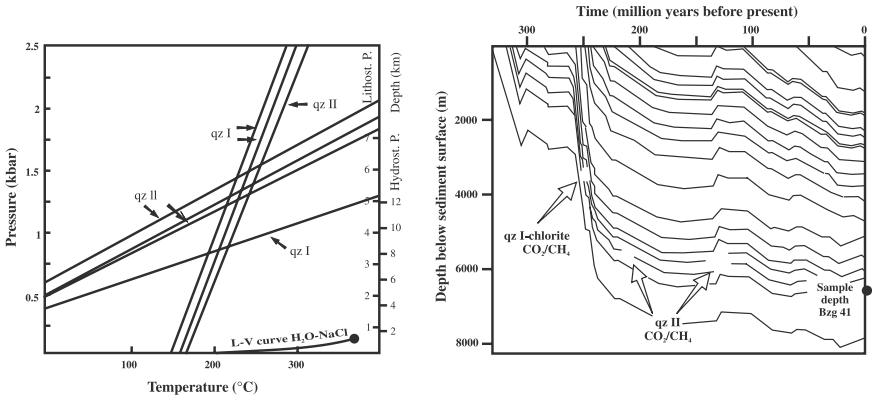

Fig. 12 Isochoric sections of aqueous and gaseous inclusions in two generations of quartz (quartz I and quartz II) hosted by Upper Carboniferous rocks from the Boizenburg 1 drill core and projection of possible time of entrapment in the burial curve

depth of about 3.3 km, whereas quartz II would have precipitated between 5 and 5.7-km depth. In first scenario, the homogenization temperatures of primary aqueous fluid inclusions in quartz I point to an enhanced heat flow during fluid migration and entrapment, considering a geothermal gradient of about 30°C/km for the host rocks. Transferring the estimated depths of quartz crystallization to the burial curves of the Boizenburg well (Fig. 12) it appears that the precipitation of quartz I was probably related to a late stage of increased subsidence and indicates an early CH_4–CO_2 migration in Upper Permian times.

During the Lower Triassic pressure conditions changed from predominantly lithostatic to predominantly hydrostatic resulting in the deposition of quartz I.

Quartz II precipitated under nearly lithostatic conditions at a depth ≥ 5–5.7 km. Therefore, it seems very likely that the migration of gas and fluids and the precipitation of quartz II can be related to the final stage of subsidence (Fig. 12).

The age relationships of fissure minerals hosted by Carboniferous sediments within the other studied wells, including those in the area of the Altmark gas field, are not as well constrained as in the Boizenburg borehole described above. Nevertheless, the isochoric sections of aqueous and gaseous inclusions (Fig. 11) always reveal pressure conditions higher than hydrostatic for fluid entrapment of CH_4–CO_2 and aqueous fluids in accordance with sample depth and burial curves under enhanced heat-flow conditions. These findings are similar to those reported for samples from wells within a NW-NNW/SE-SSE striking lineament structure in the Lower Saxony Basin (Fig. 1), where gas is produced from fractured Carboniferous reservoirs. Here, Carboniferous sandstones were uplifted due to the Cretaceous inversion by some hundreds of meters in wrench structures (Reutel et al. 1995).

In contrast, isochoric sections of highly saline H_2O–NaCl–$CaCl_2$ inclusions and co-genetically trapped N_2–CH_4 gas mixtures reveal completely different trapping conditions for most of the N_2-rich inclusions. In the eastern part of the NGB, these fluid inclusion assemblages in fissure minerals, hosted by Permian rocks or evaporites were trapped under a low-pressure regime of about 200–400 bar (Fig. 11). The observed phase transition, i.e. L → V homogenization, point to high molar volumes of the trapped gas mixtures and suggest (nearly) hydrostatic trapping conditions which can probably be related to the main stages of basin uplift (Jurassic/Cretaceous, Lower/Upper Cretaceous, Cretaceous/Tertiary boundaries). Thus, it seems very likely that the formation of gas reservoirs with high nitrogen contents was related to these stages of basin evolution.

Origin of nitrogen

The origin of nitrogen in gas reservoirs in the eastern part of the NGB is controversial (for references see Mingram et al. 2005). Chemical analysis of individual fluid inclusions hosted in a fissure calcite sample from the Schwerin 1 borehole (Table. 1, 2) proves that there to be a strong evidence for local interactions of saline brines with Permian volcanic rocks and a probable release of nitrogen from feldspar and/or mica. The thickness of the volcanic rocks in the study area often exceeds more than 1,000 m. Since the analysed N_2-bearing fluid inclusions in calcite from the Schwerin 1 borehole are absolutely unique, it seems unlikely that volcanic rocks are the main source for nitrogen in gas reservoirs of the study area. This is also indicated by the low nitrogen content in the Permain volcanic rocks which does not exceed 120 ppm (Table 3). Furthermore, even extremely altered samples do not show any significant decrease in nitrogen content. Therefore, a different source for the high nitrogen content in gas reservoirs in the eastern part of the NGB has to be considered. A sedimentary nitrogen source, i.e. shales and/or coals has been favoured in a number of previous studies (e.g. Everlien 1990; Scholten 1991; Krooss et al. 1995; Littke at el. 1995; Gerling et al. 1998; Mingram et al. 2003).

Assuming a sedimentary source for nitrogen, mainly C_{org}-rich shales with high nitrogen content can be taken into consideration because coals are less frequent in the central basin or, when present, they are of minor thickness. The release of nitrogen in the form of NH_3 and/or N_2 (depending on the oxygen fugacity of the rock) can be triggered by a thermal event (i.e. catagenesis, magmatic

intrusion) and/or by hydrothermal processes. Although nitrogen release under upper-diagenetic conditions cannot be excluded, Mingram et al. 2005 (this issue) have shown, for example, the potential for ammonium fixation in Namurian shales increases with increasing thermal maturity up to low-metamorphic conditions. On the other hand, strongly altered samples from a drill core from the central part of the NGB show a significant decrease of ammonium down to 500 ppm coupled with a shift in $\delta^{15}N$ from +3 up to +6 ‰ which suggests a release of nitrogen on a large scale (Mingram et al. 2005). WRI of brines with shales is also indicated by the sulfur isotopic composition of anhydrites in fissures hosted by Namurian shales. The anhydrites have $\delta^{34}S$ values between +3.31 and +5.61‰ and suggest mixing of SO_4^{2-}-dominant formation waters with variable amounts of dissolved biogenic sulfide derived from the shales. Intensive WRI of brines with shales would also account for the high metal content in fluid inclusions hosted in quartz II (Table. 1, 2). Therefore, an origin and release of nitrogen from C_{org}-rich shales due to WRI with saline brines is supported by fluid inclusion and stable isotope constraints.

Conclusions

Fluid inclusion studies have revealed a complex evolution of migrating fluids in the NGB. The fluid systems developed from H_2O–NaCl type during early stages of basin subsidence to H_2O–NaCl–$CaCl_2$ type during further burial. These fluids altered sedimentary strata progressively with time. Locally, fluid inclusions show evidence for strong WRI with Permian volcanic or sedimentary rocks as indicated by elevated B, K, Cs, Rb and metal contents in the trapped liquids. Fluid migration was accompanied by the migration of gases. The migration of CH_4-rich gases within the Carboniferous can be related to the main and final stages of basin subsidence. In the eastern part of the basin, gaseous inclusions in fissure minerals hosted by Permian sandstones and carbonates are generally characterized by variable N_2–CH_4 compositions but contain no CO_2. These gas mixtures were trapped at considerably lower *P*–*T* conditions than CH_4-rich inclusions within Carboniferous lithologies. Therefore, the entrapment of N_2–CH_4 inclusions seems very likely to be related to phases of tectonic uplift. The source of nitrogen is assumed to be intensive WRI of highly saline brines with Carboniferous or even older shales.

Acknowledgements This paper benefited significantly from reviews by Rudy Svennen (Leuven) and a (nearly) unknown reviewer of the International Journal of Sciences (*Geologische Rundschau*). We are indebted to EEG Berlin/Gaz de France, BEB Hannover and ExxonMobil Hannover/Celle for providing sample material. The study received financial support from the Deutsche Forschungsgesellschaft (DFG) Bonn.

Appendix

Table 4 Fluid inclusion microthermometric data

Sample	Stratigraphy	Host mineral	Type	Te	Tm	Th	Tm-hydrate	N
Northern Basin Margin								
Schleswig Z1								
Schl7	Rotliegend	Quartz	Aqueous	−73.5 to −59.6	−38.8 to −16.2	114 to 154.1	−11.3 to 16.4	30
Schl 8	Rotliegend	Carbonate	Aqueous	−74.9 to −65.2	−50.4 to −30.2	158.1 to 253.7		23
Schl 13	Visean	Carbonate	Aqueous	−72.3 to −2.5	−39.1 to + 3.4	105.1 to 146.9	−13.8 to + 15	34
Schl 19	Magmatic dyke	Quartz	Aqueous	−70.5 to −59.2	−26.1 to −24.3	148.7 to 165.3	3.1 to 8.5	19
Schl 19	Magmatic dyke	Quartz	Gaseous	~ −41	~ 0.7 to 2.5	−148.6 to −146.5		8
Schl 36	Tournaisian	Carbonate	Aqueous	−75.4 to −66.7	−39.5 to −25.8	168.1 to 257.7	0.2 to 16.6	18
Schl 36	Tournaisian	Carbonate	Aqueous	−71.4 to −56.8	−40.2 to −20.8	130.3 to 247.3		7
Central Basin								
Sample	Stratigraphy	Host mineral	Type	Te	Tm	Th	Tm-hydrate	Tm-dms	N
Vellahn 1									
V 19	Rotliegend	Carbonate	Aqueous	−70.1 to −50.6	−51.6 to −21.0	171.8 to 204.0	−39.7 to +20.0	196.7	28
V 22	Rotliegend	Carbonate	Aqueous	−58.4 to −53.8	−39.1 to −27.0	159.8 to 171.9	9.3 to 17.6		34
V 22	Rotliegend	Carbonate	Gaseous			−192.6 to −189.2			3
V 23	Rotliegend	Carbonate	Aqueous	−70.0 to −64.0	−31.0 to −26.8	164.5 to 189.3	−6.1 to +19.8		16
V 24	Rotliegend	Calcite	Aqueous	−62.5 to −55.2	−43.1 to −26.3	166.9 to 183.9	7.7 to 10.4		22

Table 4 (Contd.)

Central Basin

Sample	Stratigraphy	Host mineral	Type	Te	Tm	Th	Tm-hydrate	Tm-dms	N
V 24	Rotliegend	Calcite	Gaseous			−94.3 to −93	20 to 20.4 ?	30 ?	4
V 25	Rotliegend	Calcite	Aqueous	−58.4 to −52.4	−34.0 to −30.2	170.5 to 190.1	13.2		11
V 26	Rotliegend	Carbonate	Aqueous	−67.0 to −53.2	−39.1 to −27.0	172.2 to 191.2			12
V 27	Rotliegend	Carbonate	Aqueous	−73.3 to −68.6	−39.0 to −35.2	179.9 to 200.0	−27.5 to −26.0		22
Schwerin 1									
S 4	Rotliegend	Calcite	Aqueous	−68.0 to −59.2	∼ −20	177 to 204.5			15
S 9	Rotliegend	Calcite	Aqueous/gas.	−78.3 to −58.3	−37.3 to −32.7	208.3 to 227.7	17.0 to 21.2	171 to 180	32
S 10	Rotliegend	Calcite	Aqueous/gas.	−74.4 to −56.7	−40.6 to −33.2	210.0 to 223.4	−1.1 to +23.6	204 to 210	40
S 10	Rotliegend	Calcite	Gaseous			−194.3 to −193.6			5
S 13	Rotliegend	Calcite	Aqueous/gas.	−61.8 to −59.2	−37.2 to −33.9	205.1 to 232.7	22.7 to 25.8	168.9 to 196.6	45
S 13	Rotliegend	Calcite	Gaseous			−197.6 to −192.8			4
S 2-9	Rotliegend/volc.	Calcite/anhydr.	Aqueous	−61.4 to −60.2	−37.2 to −36.4	219.3 to 229.4		196.7	14
S 2-10	Rotliegend/volc.	Calcite/anhydr.	Aqueous	−74.3 to −68.9	−39.8 to −37.2	178.0 to 197.5			12
Eldena 1									
Ela 41	Rotliegend	Anhydrite	Aqueous	−67.0 to −64.7	−31.6 to −29.6	148.4 to 164.0	16.6 to 20.4		22
Ela 29	Rotliegend	Quartz	Aqueous	−68.6 to −66.0	−22.1 to −17.1	169.3 to 180.0			17
El H 19	Namurian	Quartz/calcite	Aqueous	−65.2 to −61.7	−25.6 to −24.0	170.2 to 174.8			6
El H 23	Namurian	Quartz	Aqueous	ND	−24.2 to −22.6	171.6 to 176.2			8
El H 23	Namurian	Quartz	Gaseous			∼ −73			4
El H 24	Namurian	Quartz	Aqueous	ND	−25.0 to −23.4	174.2 to 176.6			6
El H 24	Namurian	Quartz	Gaseous			−74 to −72.5			6
Pröttlin 1									
Pr H5	Namurian	Calcite	Aqueous	ND	−24.5 to −21.2	182.5 to 190.0			8
Pr H5	Namurian	Calcite	Gaseous			∼ −194			8
Parchim 1									
Pa 48	Rotliegend	Calcite	Gaseous			−198.2 to −197.1			4
Pa 48	Rotliegend	Calcite	Aqueous	ND	−24.2 to −22.6	171.6 to 176.2			27
Pa 1/10	Namurian	Calcite	Aqueous	−58 to −53	−35.4 to −20.8	168.7 to 192.3	−10.8 to −7.2	148.7	20
Pa 1/15	Namurian	Quartz	Aqu./gas.	−79.7 to −44.0	−10.2 to −6.3	179.1 to 225.0	13.5		24
Pa 1/15	Namurian	Quartz	Gaseous		−79.0 to −78.9	−79.7 to −69.4			11
Pa 1/15	Namurian	Calcite	Aqueous	ND	ND	202.2 to 235.7			12
Pa H16	Namurian	Quartz	Aqueous	ND	−14.4 to −6.7	165.0 to 220.7			16
Pa H16	Namurian	Quartz	Aqueous	−60.0 to −58.1	−38.0 to −35.4	179.8 to 184.9			5
Kaarßen 1									
Kaa 36	Rotliegend	Calcite	Aqueous	−54.8 to −52.5	−32.3 to −22.9	138.3 to 151.6	−13.3 to −6.6		42
Kaa 37	Rotliegend	Calcite	Aqueous	−54.3 to −52.4	−29.5 to −26.1	135.5 to 154.6	−3.1 to +3.8		29
Boizenburg									
Bzg 45	Rotliegend	Carbonate	Aqueous	−58.9 to −51.5	−37.5 to −27.3	162 to 178.5			11
Bzg 45	Rotliegend	Carbonate	Gaseous			−84.5 to −84			12
Bzg 23	Westphalian A	Quartz	Aqueous	ND	−30.0 to −25.6	155.2 to 165.0			10
Bzg 41	Namurian	uuartz I	Aqueous	−22 to −20.8	−12.5 to −6.5	165.2 to 179.5			5
Bzg 41	Namurian	Quartz I	Aqueous	ND	−40.4 to −14.4	143.3 to 157.4			29
Bzg 41	Namurian	Quartz I + II	Gaseous		−83.5 to −63.8	−63.7 to −52.7			13
Rambow									
Rmw 51	Rotliegend	Carbonate	Aqueous	−62.1 to −58.4	−40.3 to −22.1	119.8 to 154.9	−16.2 to +1.8		49

Table 4 (Contd.)

Altmark High

Sample	Stratigraphy	Host mineral	Type	Te	Tm	Th	Tm-hydrate	Tm-dms	N
Peckensen 7									
Pe 7-4	Zechstein-z1	Calcite	Gaseous			−125.3 to −109.2			6
Pe 7-4	Zechstein-z1	Calcite	Aqueous	−57.6 to −54	−32.6 to −30	86.5 to 96.8	25.7 to 27.9		12
Pe 7-3	Zechstein-z1	Calcite	Gaseous			−138 to −123.2			7
Pe 7-3	Zechstein-z1	Calcite	aqueous	−60.5	−34.8	116 to 145			3
Pe 7-2	Zechstein-z1	Fluorite	Gaseous			−129.2 to −127.8			8
Pe 7-2	Zechstein-z1	Fluorite	Aqueous	−55.7 to −53.8	−39.1 to −38.5	114.6 to 115.9	10 to 14.6		15
Pe 7-5	Namurian	Quartz	Gaseous		−85.6 to −83.2	−78.8 to −77.1			10
Pe 7-5	Namurian	Quartz	Aqueous	−40.4 to −38.6	−30.1 to −28.7	170.3 to 171.4	18.9		20
Pe 7-5	Namurian	Calcite	Gaseous		−84.5 to −84	−75.9 to −75.6			12
Pe 7-5	Namurian	Calcite	Aqueous	−53.5 to −51	−35.2 to −34.5	168.5 to 175.4			15
Pe 7-7/E1	Namurian	Quartz	Gaseous		−78.9 to −77.6	−70.3 to −65.9			7
Pe 7-7/E1	Namurian	Quartz	Aqueous	−55 to −53.5	−31.4 to −30.1	153 to 171	18.6		17
Pe 7-7/E1	Namurian	Calcite	Gaseous		−72.8 to −71.8	−62.2 to −55.3			9
Pe 7-7/E1	Namurian	Calcite	Aqueous	−31.2 to −26.9	−0.5/+18.5	130.9 to 161			18
Pe 7-7/E1	Namurian	Quartz	Gaseous		−90.1 to −88.2	−73.5 to −71.8			8
Pe 7-7/E1	Namurian	Quartz	Aqueous	−51.2 to −50.2	−32 to −28.8	163 to 172	10		14
Pe 7-7/E2	Namurian	Quartz	Gaseous		−88	−75.4			6
Pe 7-7/E2	Namurian	Quartz	Aqueous	−52	−29.4	169.3			1
Pe 7-7/E3	Namurian	Quartz	Gaseous		−86	−69.8			1
Pe 7-7/E3	Namurian	Quartz	Aqueous	−57.4	−40	152	19		3
Mellin 8									
MI 8	Rotliegend	Calcite		−69.4 to −50.4	−37.9 to −35.7	120.2 to 127.8			4
Ml 8-1	Rotliegend	Fluorite	Gaseous			−133 to −132			2
Ml 8-2	Rotliegend	Fluorite	Aqueous	−57.2 to −56.1	−22.5 to −22.4	142.5 to 146.2	6.6		7
Ml 8-3	Rotliegend	Fluorite	Gaseous			−138.1 to −136.6			4
Ml 8-4	Rotliegend	Fluorite	Aqueous	−59.2 to −50.4	−22.4 to −22	143 to 158	−7.4 to +7.2		9
Bonese 4									
Bos 4-4	Rotliegend	Calcite	Gaseous			−125			1
Bos 4-4	Rotliegend	Calcite	Aqueous	−36	−27	144 to 146			3
Bos 4-22	Rotliegend	Calcite	Gaseous			−140 to −136			4
Bos 4-22	Rotliegend	Calcite	Aqueous	−52.1	−33.4	154			1

Flechtingen-Calvörde Block

Sample	Stratigraphy	Host mineral	Type	Te	Tm	Th	Tm hydrate	Tm-dms	N
Eiche-quarry									
Eiche 6.S	Rotliegend/volc.	Quartz	Aqueous	−76.3 to −66	−39.6 to −28.4	130.5 to 162.2			20
Flechtingen–quarry									
Quartz 1	Rotliegend/volc.	Quartz	Aqueous	−76.4 to −41.4	−39.8 to −24.4	120.8 to 188.8	−1.1 to + 10.5		51
Quartz 2	Rotliegend/volc.	Quartz	Aqueous	−73.8 to −62.4	−38.1 to 23.8	112.2 to 213.5	−2.6 to −0.2		28
Quartz 3	Rotliegend/volc.	Quartz	Aqueous	−75.1 to −4	−37.5 to + 0.5	112.5 to 191.8			34
Quartz 4	Rotliegend/volc.	Quartz	Aqueous	−72.1 to −63.3	−39.1 to + 0.5	136.8 to 210.7			28
Utmöden 14									
UTM-14	Zechstein-z1	Fluorite	Aqueous	−88.5 to −65.3	−39.5 to −25.8	69.5to207.4	−7.8 to + 12.1		79

Table 4 (Contd.)

Flechtingen-Calvörde Block

Sample	Stratigraphy	Host mineral	Type	Te	Tm	Th	Tm hydrate	Tm-dms	N
UTM 14-G	Zechstein-z1	Fluorite	Gaseous			−140/−137			5
UTM 14-G	Zechstein-z1	Fluorite	Aqueous	−55.5 to −53.6	−28.2 to 26.9	120 to 136.9			12
UTM 14-1	Zechstein-z1	Fluorite	Gaseous			−141/−137.8			9
UTM 14-1	Zechstein-z1	Calcite	Aqueous	−56.7 to −54.3	−25.1 to 23.9	125.2 to 134.8			15

Southeastern Basin Area

Sample	Stratigraphy	Host mineral	Type	Te	Tm	Th	Tm-hydrate	Tm-dms	N
Brandenburg E Br 1Eh/68									
Br 106	Visean	Quartz	Aqueous	< −40	−34.0/−32.0	74.9/106.8	−21.2/−16.6		11
Br 106	Visean	Quartz	Gaseous			−142/−140			3
Br 107	Visean	Quartz	Aqueous	−67.0/−63.0	−34.9/−31.2	128.5/137.9			24
Br 110	Visean	Carbonate	Aqueous			127.6/134.2			6
Buchholz E BzP 6/62									
BzP 22	Stephanian	Calcite	Gaseous			−195.0/−177.0			3
BzP 23	Devonian	Quartz	Aqueous		−2.5/0.8	115 to 165			6
BzP 25	Devonian	Quartz	Aqueous		−23.0/−20.5	127.4 to 153.6	−1.2/1.8		17
BzP 29	Devonian	Quartz	Aqueous	−29/−19	−2.8/−2.0	123.3 to 167.2			15
Ragösen RgoeBg 1/72									
Rgoe 74	Zechstein-z1	Calcite	Aqueous	−64.0/−61.0	−38.2/−34.3	165.4/185.1	11.7/12.6		11
Rgoe 74	Zechstein-z1	Calcite	Gaseous			−196.4/−195.1			3
Rgoe 79	Zechstein-z1	Anhydrite	Aqueous	−62.0/−59.5	−33.4/−31.3	105.3/119.5			12
Rgoe 80	Zechstein-z1	Calcite	Aqueous	−63.0/−60.0	−33.8/−31.4	132.0/157.5			10
Rgoe 82	Zechstein-z1	Dolomite	Aqueous		−37.2/−35	67.5/68.6	26.3/27.7		3
Schlepzig Sep 2/65 - Sep 6/81									
Sep6 117	Zechstein-z2	Carbonate	Aqueous			101.7 to 103.8	10.3	117.6	25
Sep6 119	Zechstein-z2	Carbonate	Aqueous	−80.4/−42.0	−46.3/−42.0	88.1 to 120.2	8.4/22.2	118.0/126.4	25
Sep2 66	Zechstein-z1	Carbonate	Gaseous			−133.6/−129.4			6
Sep2 68	Zechstein-z1/T	Carbonate	Gaseous			−85.0/−80.0			4
Sep2 68	Zechstein-z1/T	Carbonate	Aqueous	−60 ?		131.3 to 139/211	0		5
Gröditzsch E Gdc 1/82									
Gdc 36	Zechstein-z2	Calcite	Aqueous	−67.8/−61.8	−38.1/−36.0	94.4/122.2	14.0/19.8	122.2/134.0	11
Gdc 38	Zechstein-z2	Calcite	Aqueous	−81.0/−60.0	−35.7/−19.8	69.9/99.4	−6.5/−4.6		19
Gdc 40	Zechstein-z1	Carbonate	Gaseous			−124.0/−120.6			21
Gdc 41	Zechstein-z1	Carbonate	Gaseous			−121.8/−116.9			8
Lübben E Ln 102/63									
Lü 100	Zechstein-z2	Calcite	Aqueous	ND	ND	57.3 to 67.3			8
Burg E Bu 10/74									
Bg 58	Rotliegend	Calcite	Gaseous			−29.8/−25.4			4
Staakow E StwLn 12/61									
Stw 96	Rotliegend	Carbonate	Aqueous	−53/−49	−22.3/−21.1	112.3 to 137.8			19
Leibsch E Lbc 2/81									
Lbc 11	Zechstein-z1	Anhydrite	Gaseous			−149.4/−133.0			19
Lbc 12	Zechstein-z1	Calcite	Gaseous			−137.0/−135.9			6
Rüdersdorf RüdFu 13/61									
Rüd 86	Zechstein-z1	Calcite	Aqueous/gas.			−138.6			1

Table 4 (Contd.)

Southeastern Basin Area

Sample	Stratigraphy	Host mineral	Type	Te	Tm	Th	Tm-hydrate	Tm-dms	N
Rüd 86	Zechstein-z1	Calcite	Aqueous/gas.	−46	−22/−17	decrepitated			6
Rüd 86	Zechstein-z1	Calcite	Aqueous	−71.2/−68.0	−36.7/−26.1	86.0/111.0			13

Mid-German Crystalline High

Sample	Stratigraphy	Host mineral	Type	Te	Tm	Th	Tm-hydrate	Tm-dms	N
Schadewalde E She 2/75									
She I	Zechstein-z1	Calcite	Gaseous			−81.2/−80.8			2
She VI	Zechstein-z1	Calcite	Aqueous	−62.0/−57.0	−25.0/−20.5	108.2/112.7			6
She IX	Rotliegend	Calcite	Gaseous		−70.0/−65.0	−30.0/−29.0			2
She X	Stefanian ?	Calcite	Aqueous	−58.0/−53.5	−23.0/−20.8	120.2/125.6			6
She XI	Stefanian ?	Quartz	Gaseous		−122.6/−100.9	−74.5/−58.8			7
She XI	Stefanian ?	Quartz	Aqueous	−56.0/−48.5	−25.2/−22.4	115.5/160.5			22
She XII	Stefanian ?	Quartz	Gaseous			−50.0/−36.0			8
She XIII	Stefanian C	Quartz	Aqueous	−61.0/−56.0	−23.8/−22.1	118.6/160.1			17
She XIII	Stefanian C	Quartz	Gaseous			−85.0/−90.0			3
She XV	Stefanian C	Quartz	Gaseous			−88.8			1
She XV	Stefanian C	Quartz	Aqueous	−55.5/−51.0	−22.6/−21.2	120.3/150.2			24
She XVIII	Stefanian C	Quartz	Aqueous	−60.0/−56.0	−22.4/−20.5	123.4/143.4			12
Drebkau Drk 1/63									
Drk 64	Carboniferous	Carbonate	Gaseous		−180.7	−92.2			2
Drk 65	Carboniferous	Quartz	Gaseous			−107.5/−95.8			4
Drk 65	Carboniferous	Quartz	Aqueous	−67.0/−58.9	−45.0/−24.0	96.6/124.9	−25.7/−17		5
Drk 66	Carboniferous	Quartz	Aqueous	−31.8/−29.0	−1.4/0.0	242.2/295.1			14
Drk 66	Carboniferous	Quartz	Gaseous		−183.0/−181.0	−130.6/−97.3			14

z1 Werra Formation, *z2* Stassfurt Formation, majority of z1 and z2 samples are taken from the anhydrite and the carbonate members, *z1T* Kupferschiefer; *volc.* volcanic rock; stratigraphic classification of the Carboniferous part of the Drebkau well is insecure. *ND* not determined.

References

Bandlowa T (1998) Erdgasführung im Karbon-Perm-Trias-Komplex der mitteleuropäischen Senke. Geol Jb A 151:3–65

Banks DA, Giuliani G, Yardley BDW, Cheilletz A (2000) Emerald mineralisation in Colombia: fluid chemistry and the role of brine mixing. Miner Deposita 35:699–713

Banks DA, Boyce AJ, Samson IM (2002) Constraints on the origins of fluids forming Irish Zn-Pb-Ba deposits: evidence from the composition of fluid inclusions. Econ Geol 97:471–480

BGR, BGS, GEUS, TNO, PGI (1998) NW European Gas Atlas. In: Lokhurst (ed), ISBN 90–72869–60–5

Brown PE, Hagemann SG (1994) MacFlinCor: a computer program for fluid inclusion data reduction and manipulation. In: De Vivo B, Frezotti ML (eds) Fluid Inclusions in minerals: methods and applications. IMA Short C, pp 231–250

Davis DW, Lowenstein TK, Spencer RJ (1990) Melting behavior of fluid inclusions in laboratory-grown halite crystals in the systems NaCl–H_2O, NaCl–KCl–H_2O, NaCl–$MgCl_2$–H_2O, and NaCl–$CaCl_2$–H_2O. Geochim Cosmoschim Acta 54:591–601

Davisson ML and Criss RE (1996) Na–Ca–Cl relations in basinal fluids. Geochim et Cosmochim Acta 60:2743–2752

Everlien G (1990) Das Verhalten des in Mineralen gebundenen Stickstoffs während der Diagenese und Metamorphose von Sedimenten. PhD Thesis, TU Braunschweig, pp 1–88

Fontes JC, Matray JM (1993) Geochemistry and origin of formation brines from the Paris Basin, France. 1. Brines associated with Triasssic salts. Chem Geol 109:149–175

Gerling P, Kockel F, Krull P (1999) Das Kohlenwasserstoffpotential des Präwestfals im Norddeutschen Becken. DGMK Forschungsb 433:1–107

Gerling P, Lokhorst A, Nicholson RA, Kotarba M (1998) Natural gas from Pre-Westphalian sources in Northwest Europe – a new exploration target. – Int. Gas Research Conf., Proceedings, 219–229, San Diego

Günther D, Audetat A, Frischknecht R, Heinrich CA (1998) Quantitative analysis of major, minor and trace elements in fluid inclusions using laser ablation inductively coupled plasma mass spectrometry. J Anal Atom Spec 13(4):263–270

Goldstein RH (2001) Fluid inclusions in sedimentary and diagenetic systems. Lithos 55:159–193

Goldstein RH, Reynolds TJ (1994) Systematics of fluid inclusions in diagenetic minerals. SEPM Short C 31, pp 1–199

Heinrich CA, Pettke T, Halter WE, Aigner-Torres M, Audétat A, Günther D, Hattendorf B, Bleiner D, Guillong M, Horn I (2003) Quantitative multi-element analysis of minerals, fluid and melt inclusions by laser-ablation inductively-coupled-plasma mass-spectrometry. Geochim Cosmochim Acta 67:3473–3496

Hoth P (1997) Fazies und Diagenese von Präperm-Sedimenten der Geotraverse Harz - Rügen. Schriftenr Geowiss 4:1–139

Krooss BM, Littke R, Müller B, Frielingsdorf J, Schwochau K, Idiz EF (1995) Generation of nitrogen and methane from sedimentary organic matter: implications on the dynamics of natural gas accumulations. Chem Geol 126:291–318

Littke R, Krooss BM, Idiz EF, Frielingsdorf J (1995) Molecular nitrogen in natural gas accumulations: generation from sedimentary organic matter at high temperatures. Am Assoc Pet Geol Bull 79:410–430

Lüders V, Möller P (1992) Fluid evolution and ore deposition in the Harz Mountains (Germany). Eur J Mineral 4:1053–1068

Lüders V, Stedingk K, Franzke HJ (1993) Review of geological setting and mineral paragenesis. In: Möller P, Lüders V (eds) Formation of hydrothermal vein deposits—a case study of the Pb-Zn, barite and fluorite deposits of the Harz Mountains, Mono Ser Min Dep 30:5–11

Lüders V, Hoth P, Reutel C (1999) Fluid- and gas migration in the eastern part of the North German Basin. Terra Nostra 99/6:193–195

Mingram B, Hoth P, Lüders V, Harlov D (2005) The significance of fixed ammonium in Paleozoic sediments for the generation of nitrogen rich natural gases in the North German Basin (NGB). This issue

Nielsen H (1979) Sulfur isotopes in nature. In: Jäger E, Hunziker J (eds) Lectures in isotope geology. Springer, Berlin Heidelberg New York, pp 283–312

Ohmoto H (1972) Systematics of sulfur and carbon isotopes in hydrothermal ore deposits. Econ Geol 67:551–579

Ohmoto H, Lasaga AC (1982) Kinetics of reactions between aqueous sulfates and sulfides in hydrothermal systems. Geochim Cosmochim Acta 46:1727–1745

Ohmoto H, Rye RO (1979) Isotopes of sulfur and carbon. In: Barnes HL (ed) Geochemistry of hydrothermal ore deposits, 2nd edn. Wiley, New York, pp 509–567

Pettke T, Halter WE, Webster JD, Aigner-Torres M, Heinrich CA (2004) Accurate quantification of melt inclusion chemistry by LA-ICPMS: A comparison with EMP and SIMS and advantages and possible limitations of these methods. Lithos 78:333–361

Reutel C, Lüders V (1998) Fluid-Evolution und Gasmigration im südlichen Randbereich des Nordostdeutschen Beckens – Untersuchungen an Flüssigkeitseinschlüssen in Kluftmineralisationen und im Werra-Anhydrit. Geol Jb A 149:169–183

Reutel C, Lüders V, Hoth P, Idiz EF (1995) Gas migration and accumulation along lineament structures – Lower Saxony Basin (NW Germany). Bol Soc Espan Min 18:205–206

Rieken R (1988) Lösungs-Zusammensetzung und Migrationsprozesse von Paläo-Fluidsystemen in Sedimentgesteinen des Nordwestdeutschen Beckens. PhD Thesis, Univ Göttingen, GAGP 37, pp 1–116

Rieken R, Gaupp R (1991) Fluideinschluß-Untersuchungen an Sandsteinen des Gasfeldes Thönse. Nds Akad Geowiss Veröfftl 6:68–99

Roedder E (1984) Fluid inclusions. Mineral Soc Am Rev Mineral 12:1–644

Schmidt Mumm A, Wolfgramm M (2004) Fluid systems and mineralisation in the North German and Polish Basin. Geofluids 4:315–328

Scholten SO (1991) The distribution of nitrogen isotopes in sediments. Geol Ultraiectina 81:1–101

Spencer RJ, Møller N, Weare JH (1990) The prediction of mineral solubilities in natural water: A chemical equilibrium model for the Na–K–Ca–Mg–Cl–SO_4–H_2O system at temperatures below 25°C. Geochim Cosmochim Acta 54:575–590

Stedingk K, Ehling B-C, Knoth W, Germann K, Schwab M (1995) Epigenetic mineralizing processes in the Northeastern Rhenohercynian Belt (Harz Mountains, Flechtingen-Rosslau Block). In: Pašava J, Kříbek B, Žák K (eds) Mineral Deposits: from their origin to their environmental impacts, pp 79–82

Thiéry R, Vidal J, Dubessy J (1994) Phase equilibria modelling applied to fluid inclusions. Liquid-vapour eqilibria and calculation of the molar volume in the CO_2–CH_4–N_2system. Geochim Cosmochim Acta 58:1073–1082

Verma SP, Santoyo E (1997) New improved equations for Na/K, Na/Li and SiO2 geothermometers by outlier detection and rejection. J Volcanol Geotherm Res 79:9–23

Wolfgramm M (2002) Fluidentwicklung und Diagenese im Nordostdeutschen Becken – Petrographie, Mikrothermometrie und Geochemie stabiler Isotope. PhD thesis, Univ Halle, pp 1–170